# QUANTIFYING EOCENE AND MIOCENE EXTENSION IN THE SEVIER HINTERLAND IN NORTHEASTERN NEVADA

By

JENNIFER N. GIFFORD

A THESIS PRESENTED TO THE GRADUATE SCHOOL
OF THE UNIVERSITY OF FLORIDA IN PARTIAL FULFILLMENT
OF THE REQUIREMENTS FOR THE DEGREE OF
MASTER OF SCIENCE

UNIVERSITY OF FLORIDA

2008

To my mother, who greatly encouraged me in my pursuit of science

ACKNOWLEDGMENTS

I wish to thank my Advisor Dr. David Foster for his help and patience. I also wish to thank my committee members for their guidance and helpful reviews of my thesis material. I especially wish to thank Shawn J. Malone for his endless assistance. I also wish to thank Warren Grice and Misty Stroud for their assistance in analysis procedures. Richard McKenzie for all of his help with my figures. Finally, I wish to thank my family for their un-ending love and support.

TABLE OF CONTENTS

page

ACKNOWLEDGMENTS ..... 4

LIST OF TABLES ..... 6

LIST OF FIGURES ..... 7

ABSTRACT ..... 8

CHAPTER

1 INTRODUCTION ..... 10

2 REGIONAL GEOLOGY ..... 12

3 $^{40}Ar/^{39}Ar$ THERMOCHRONOLOGY ..... 16

Previous Thermochronology ..... 16
$^{40}Ar/^{39}Ar$ Thermochronology Results ..... 18
Biotite ..... 19
Muscovite ..... 21

4 DISCUSSION ..... 30

Eocene Exhumation of the Ruby Mountains Metamorphic Core Complex defined by $^{40}Ar/^{39}Ar$ Thermochronology ..... 30
Constraints on the Timing of the Onset of Extension ..... 31
Constraints on the Detachment Slip Rate ..... 32

5 CONCLUSIONS ..... 41

APPENDIX $^{40}Ar/^{39}Ar$ THERMOCHRONOLOGY METHODS ..... 42

Sample Preparation and Irradiation ..... 42
$^{40}Ar/^{39}Ar$ Analytical Instrumentation and Procedures ..... 43

LIST OF REFERENCES ..... 45

BIOGRAPHICAL SKETCH ..... 48

LIST OF TABLES

Table page

3-1 Summary of previous $^{40}Ar/^{39}Ar$ thermochronology research. ....26

3-2 Summary of $^{40}Ar/^{39}Ar$ thermochronology from the Ruby Mountains metamorphic core complex ....28

3-3 Summary of level of chloritization of samples from the Ruby Mountains metamorphic core complex ....29

LIST OF FIGURES


Figure page

2-1 Location map of the Ruby Mountains metamorphic core complex (blue), the Elko-Carlin gold trend (yellow), as well as the Antler and Sevier thrust belts. .....15

3-1 Biotite $^{40}Ar/^{39}Ar$ thermochronology step-heating mineral age ranges for samples collected from the Ruby Mountains Metamorphic Core complex along two separate transects. All ages are weighted plateau cooling ages calculated from three or more heating steps. .....23

3-2 Muscovite $^{40}Ar/^{39}Ar$ thermochronology step-heating mineral age ranges for samples collected from the Ruby Mountains Metamorphic Core complex along two separate transects. All ages are weighted plateau cooling ages calculated from three or more heating steps. .....24

4-1 Simplified geologic map showing mineral cooling ages from samples, collected along transects across Lamoille Canyon and the East Humboldt Range, using $^{40}Ar/^{39}Ar$ thermochronology (2σ). .....35

4-2 Plot of sample calculated ages vs. the altitude at which samples were collected. .....36

4-3 All of the mica $^{40}Ar/^{39}Ar$ thermochronology ages from the Lamoille Canyon transect were plotted versus their distance along slip direction. .....37

4-4 Mica $^{40}Ar/^{39}Ar$ thermochronology ages versus distance in slip direction from the Lamoille Canyon transect, younger age grouping. A regression was calculated for the sample set. .....38

4-5 Mica $^{40}Ar/^{39}Ar$ thermochronology ages versus distance in slip direction from the Lamoille Canyon transect, older age grouping. A regression was calculated for the sample set. .....39

4-6 All of the mica $^{40}Ar/^{39}Ar$ thermochronology ages from the East Humboldt Range transect were plotted versus their distance along slip direction. .....40

Abstract of Thesis Presented to the Graduate School
of the University of Florida in Partial Fulfillment of the
Requirements for the Degree of Master of Science

QUANTIFYING EOCENE AND MIOCENE EXTENSION IN THE SEVIER HINTERLAND IN NORTHEASTERN NEVADA

By

Jennifer N. Gifford

May 2008

Chair: David A. Foster
Major: Geology

Rocks exposed in the Ruby-East Humboldt metamorphic core-complex, NE Nevada, provide a guide for reconstructing the pre-Eocene crustal structure in the hinterland of the Sevier Orogen. These rocks occupy the footwall of a major west-dipping normal-sense shear system that may extend ~ 50 km further west under part of the mineralized Carlin trend. Previous thermochronologic studies showed mineral cooling ages from the Ruby Mountains core complex generally grow younger to the WNW, in the direction of fault slip. $^{40}Ar/^{39}Ar$ biotite and muscovite analyses from transects in the direction of slip on the Ruby detachment give apparent ages between ca. 31 and 21 Ma and are, therefore, consistent with the previous K-Ar data in showing a decrease in cooling age from east to west. These data indicate rapid cooling due to exhumation of the footwall of the detachment started at about 23 Ma. $^{40}Ar/^{39}Ar$ data from muscovite and biotite along transects across Lamoille Canyon and the East Humboldt Range give apparent ages of ca. 33–31 Ma in the eastern part of the footwall and ca. 25–20 Ma in the western part of the footwall. The ca. 33–31 Ma apparent ages may indicate an Oligocene phase of extension at a poorly-defined rate of 4.5 +6.7/-1.9 km/m.y. A change in slope of the mica age vs. slip distance relationship at ca. 23 Ma suggests that extension began at that time. The

gradient in mica cooling ages to the west of the break in slope of this relationship suggests a slip rate of 4.2 ± 3.8 km/m.y.

# CHAPTER 1
# INTRODUCTION

Metamorphic core complexes are important geological features in the North American Cordillera, both for the glimpse they provide into the middle crust and the valuable tectonic information they contain. These complexes occur in a long belt, from southern Canada to northern Mexico in what was formerly crust thickened by Mesozoic and Cenozoic orogenic events (Coney, 1980). Core complexes develop when low-angle detachment faults exhume middle-crustal metamorphic rocks in the footwall of the fault. These complexes have been the subject of numerous studies (e.g., Armstrong and Ward, 1991; Dallmeyer et al., 1986; Howard, 1980; Howard, 2003; McGrew and Snee, 1994; Snoke, 1980), but the timing and significance of many remain uncertain. The metamorphic core complex exposed in the Ruby-East Humboldt Range is of particular interest. This complex is marked by deformed and migmitized upper amphibolite facies metamorphic rock and associated igneous bodies unroofed by slip on the main detachment. The Ruby-East Humboldt core complex occupies a central position in the hinterland region of the Sevier Orogen (e.g., Howard, 2003). This paper examines the timing and rate of Cenozoic extension and thinning of the lower crust in the Ruby Mountains metamorphic core complex via high and low temperature thermochronology ($^{40}Ar/^{39}Ar$) on rocks within structurally controlled transects.

**Metamorphic Core Complex:** Core complexes form as middle-crustal metamorphic rocks are exhumed during rapid extension, commonly in the footwall of a detachment fault. The rocks in the footwall of the detachment fault are uplifted through a progression of metamorphic facies and deformation mechanisms, resulting in a characteristic sequence of structures. The movement zone is folded as the result of the bowing upwards of the lower crust to form a broad basement culmination, and is driven by isostatic rebound due to tectonic denudation (Wernicke and Axen,

1988). Lister and Davis (1989) state that the formation of metamorphic core complexes is driven by extensional stresses in the upper crust. Three primary models explaining the deformation leading to the formation of metamorphic core complexes are noted by Brun et al. (1994). These models are the simple shear model, in which low angle detachments accommodate extension (Wernicke, 1981; Wernicke, 1985), the rotated normal fault model involving the formation of high angle normal faults which subsequently rotate to a low dip and cease to be active slip surfaces (Buck, 1988; Wernicke and Axen, 1988), and the domino (tilted block) model which postulates straight faults bounding rotating crustal blocks (Angelier and Coletta, 1983; Davis, 1983). Lister and Davis (1989) address the strengths and weaknesses of the broad mechanisms, and support a multiple detachment model. During the evolution of a metamorphic core complex, it is necessary to have multiple generations of detachment faults all splaying from an original master fault, or from a controlling movement zone at depth. The most recently active detachment fault is the youngest in a succession of faults that progressively remove lower portions of the upper plate, eating their way upwards through the overlying sequences. The detachment faults presently observed in the metamorphic core complexes (e.g., Ruby Mountains) are relatively young, and are only the last in a succession of low-angle normal faults that carve through the upper crust at the upward terminations of major, shallow-dipping, ductile shear zones in the extending Cordilleran orogen (Chery, 2001).

# CHAPTER 2
# REGIONAL GEOLOGY

By the Neoproterozoic (~ 600 Ma), the western margin of North America had developed into a passive continental margin (Burchfiel et al., 1992). This margin was characterized by marine and non-marine clastic sedimentary rocks, interbedded with carbonates in a westward thickening wedge (Burchfiel et al., 1992). These rocks were later modified by Phanerozoic orogenic events. The first Phanerozoic orogenic event is referred to as the Antler orogeny. This phase is characterized by late Neoproterozoic to upper Devonian shelf sequences thrust eastward ~ 200 km onto the edge of the North American craton (Roberts et al, 1958; Poole et al, 1992). Numerous thrust faults cut across the area affected by the Antler orogeny, leading some authors to interpret the terrane as an accretionary complex (Oldow, 1984). The basal thrust is preserved today as the Roberts Mountain thrust (Burchfiel et al., 1992). The next major contractional event is referred to as the Sonoma orogeny. In central Nevada, the Sonoma orogeny was characterized by the eastward thrusting of the Havallah assemblage over the western elements of the Antler orogeny along the Gloconda thrust fault (Burchfiel et al., 1992). This event occurred in the latest Paleozoic to earliest Triassic (Burchfiel et al., 1992). In the Late Jurassic a further pulse of compression resulted in the Nevadan orogeny; however, the causes of this contractional event are uncertain (Burchfiel et al., 1992). From the Early to Late Cretaceous, further shortening and eastward thin-skinned thrusting define the Sevier orogeny (Burchfiel et al., 1992). Thrusting and metamorphism associated with this event ended ~70 Ma (Burchfiel et al., 1992). Some estimates place the thickness of the crust affected by the Sevier orogeny as thick as 60 to 70 km in Nevada (Burchfiel et al., 1992).

The tectonic character of the Cordilleran margin changed during the Cenozoic. The Mesozoic-Cenozoic transition was marked by continued shortening and crustal thickening

related to the Laramide orogeny and shallow-angle subduction of the Farallon slab (Sonder and Jones, 1999). During the late Eocene/early Oligocene, the Farallon slab began to roll back and peel away from its coupling with the bottom of the North American lithosphere (Humphreys, 1995). The rollback of the subducting slab allowed hot asthenospheric material to come into contact with metasomatized lithospheric mantle, promoting partial melting (Armstrong & Ward, 1991). Sonder and Jones (1999) suggest that this heat was transferred to the crust above the rolling slab, leaving it mechanically weak. A second consequence of the change in plate boundary conditions was a gradual relaxation of compressive forces from the plate boundary (Liu, 2001). As coupling between the North American and Farallon plates diminished due to slab rollback, so did the force driving thickening. Liu (2001) suggests that this relaxation of stress on the thickened crust of Eastern Nevada allowed for a change from shortening to gravitationally driven extension. Large metamorphic core complexes formed throughout southern Idaho and eastern Nevada in the 40–25 Ma time interval (Armstrong and Ward, 1991), and can be associated with both ignimbrite magmatism and the gravitational collapse of thickened crust.

**The Ruby Mountains Metamorphic Core Complex:** Howard (2003) divides northwestern Nevada into three broad tectonic elements: the hinterland of the Sevier fold and thrust belt, the Ruby-East Humboldt metamorphic core complex, and the Elko-Carlin domain. The Ruby-East Humboldt complex (Figure 2-1) exposes metamorphosed Paleozoic strata, as well as smaller areas of Proterozoic and possibly Archean rock (Howard, 2003). These metamorphic units were unroofed during the Tertiary via extensional normal faulting, which also caused mylonitization and overprinted prior metamorphic features (Howard, 2003). Metamorphic conditions in the Ruby and Humboldt ranges peaked at upper amphibolite facies,

with lower-grade facies occurring to the east and south (Howard, 2003). Snoke (1980) provides further divisions for the lithologies present in the Ruby Mountains, dividing them between the metamorphic core, unmetamorphosed Paleozoic sedimentary units exposed by a low angle fault system, and Tertiary sedimentary and volcanic units. Granitic rock forms a significant volume of the Ruby Mountains complex as well, manifested as dikes, sills, and irregular masses, commonly of two-mica pegmatitic granite (Howard, 1980). The Sevier fold and thrust belt exposes 10 to 13 km of siliciclastic and carbonate miogeoclinal strata, Neoproterozoic to early Mesozoic in age, east of the Ruby mountains (Howard, 2003). West of the Ruby Mountains in the Elko-Carlin domain, deep water strata were thrust over the miogeoclinal shelf units during a series of shortening events during the Paleozoic and Mesozoic (Howard, 2003). Backthrusting in the Elko-Carlin domain is suggested by overturned folds in several localities (Howard, 2003). In addition to these three tectonic elements, the region also exposes numerous Jurassic and early Cretaceous igneous intrusions, with late Cretaceous granites emplaced into deeper crustal levels of the metamorphic core complex (Howard, 2003).

The deep crustal rocks exposed in the Ruby-East Humboldt metamorphic core complex provide a guide for reconstructing Eocene crustal structure in northeastern Nevada (Howard, 2003). The exposed rocks from the core complex are in the footwall of a west-dipping normal-sense shear system (Howard, 2003). It has been proposed that these rocks may have underlain the Piñon and Adobe Ranges, ~ 50 km to the west, before Tertiary extension (Howard, 2003). Eocene events in the Elko-Carlin region included widespread magmatic intrusions, normal faulting, an elevated geothermal gradient from crustal thinning, and development of lacustrine deposits in active structural basins (Howard, 2003).

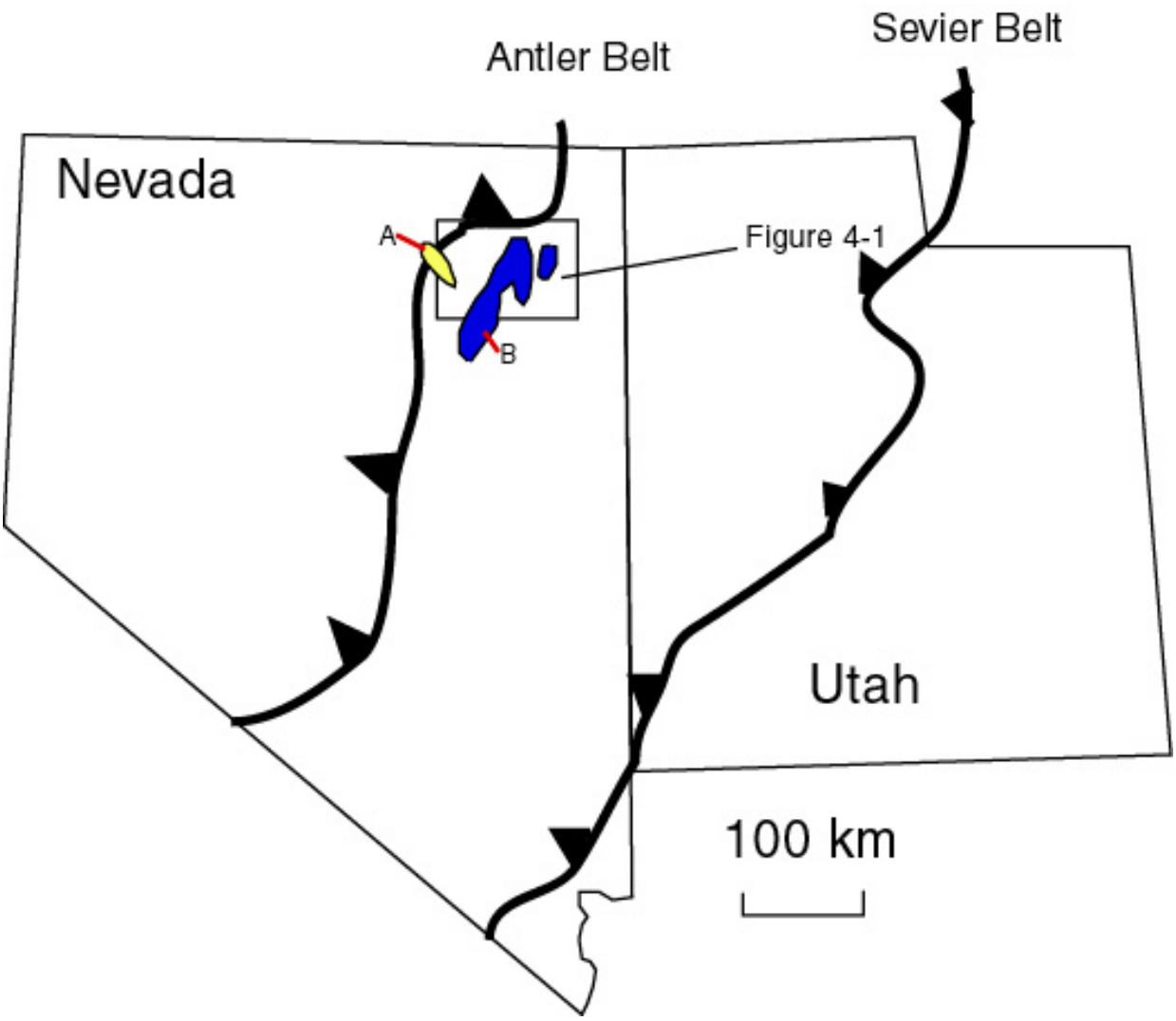


Figure 2-1. Location map. A) the Elko-Carlin gold trend. B) Ruby Mountains metamorphic core complex.

# CHAPTER 3
# $^{40}Ar/^{39}Ar$ THERMOCHRONOLOGY

## Previous Thermochronology

Despite the numerous studies of Eocene extension in the Elko-Carlin region, a clear picture of the setting and tectonics has not been formed. Evidence for Eocene extension within the high-grade metamorphic rocks of the Ruby Mountains comes mainly from $^{40}Ar/^{39}Ar$ dating of hornblende, which yielded discordant age spectra that suggested cooling during the late Eocene era (McGrew and Snee, 1994). The hornblende data are not entirely satisfactory because these data are discordant, and they can be interpreted in different ways. As shown by Howard (2003), extensive lacustrine deposits record a large Eocene lake and wetland system, which may suggest an early Tertiary phase of extension.

Mineral cooling ages obtained by $^{40}Ar/^{39}Ar$ thermochronology can be used to constrain the cooling and exhumation histories of highly extended terranes such as metamorphic core complexes (e.g., Foster and John, 1999; Stockli, 2005). Previously available thermochronological data relevant to the exhumation and cooling history of the Ruby Mountains Metamorphic Core Complex produced apparent ages ranging from the Oligocene to the earliest Miocene. These data are summarized in Table 3-1. These ages are interpreted to record cooling through the argon closure interval for biotite, which is about 350-280 at about °C depending on cooling rate (McDougall and Harrison, 1999).

Cooling ages given by mica K-Ar and apatite fission-track data from the Ruby Mountains core complex generally grow younger in the "west-northwest direction of extensional unroofing" (McGrew and Snee, 1994). Analyses reported by McGrew and Snee (1994), from 3 muscovites and 5 biotites yield apparent ages between 21.9 ± 0.2 Ma and 26.7 ± 0.1 Ma. They also determined that at ca. 20 Ma, rapid cooling occurred through the temperature interval of

approximately 300°C to below 100°C. The K-Ar biotite apparent ages indicate the time at which the sample passed through the argon retention isotherm or partial retention interval. The closure temperature for biotite is dependant on cooling rate, but generally varies between 280 and 350°C (McDougall and Harrison, 1999). The age progression of younger ages to the west can be interpreted to suggest the rate of progressive westward unroofing and cooling of the core complex, or an east-tilted oblique section through a zone of partial argon retention.

Foster and John (1999) showed that if mineral cooling ages represent quenching by progressive unroofing of an isotherm beneath an extensional shear zone, an approximate rate of lateral cooling and detachment slip can be obtained by inverting the rate of lateral age change. This inversion would indicate Oligocene and early Miocene exhumation of a westward moving hanging wall at a rate of 1 to 2 km/m.y. The westward-younging cooling age patterns, if they are combined with older mica cooling ages from exposures on the eastern side of the core complex, indicate prolonged extensional exhumation beginning in the early Tertiary era (McGrew and Snee, 1994). If age-progression data were found to suggest that the metamorphic core moved cumulatively 30–40 km east below its hanging wall over approximately 20–30 m.y., the core would previously have been to the west, underneath the valley along the east margin of the Adobe and Piñon ranges.

This apparent displacement rate calculated from the previously published data is several times slower than those reported for core complexes in the Raft River and Snake ranges, and the Colorado River extensional corridor (Miller et al., 1999; Foster and John, 1999; Wells et al., 2000; Carter et al., 2004), but similar to those from core complexes in the northern Rocky Mountains (Grice, 2006). Extension rates in many other areas of the Basin and Range province

accelerated markedly about 15–17 Ma, as determined by fission-track dating of apatite (Miller et al., 1999, Carter et al., 2004).

Dallmeyer et al., (1986) obtained $^{40}Ar/^{39}Ar$ and K-Ar ages from biotite samples in the mylonite zone located in the Northern Ruby Mountains, $^{40}Ar/^{39}Ar$ for two samples in Lamoille Canyon, and $^{40}Ar/^{39}Ar$ for biotite samples located in the South-Eastern section of the East Humboldt Range. In the East Humboldt Range outside of the mylonite zone, apparent ages ranged from ~ 32 to 33 Ma. Within the mylonite zone ranging down into the Northern Ruby Mountains, $^{40}Ar/^{39}Ar$ ages were younger but slightly more widespread, ranging from ~ 22 to 27 Ma. In Lamoille Canyon biotite from a non-mylonitic magmatic core rock yielded an age of 25.3 ± 0.7 Ma. Further west towards the opening of Lamoille Canyon and nearer to the detachment fault, a biotite from within the mylonite resulted in an age of 20.8 ± 0.5 Ma. Dallmeyer et al. (1986) hypothesized that cooling began by ~ 45 Ma and that the rocks reached temperatures below 300°C by 20 Ma.

Dokka et al., (1986) published fission track data for apatites, sphenes, and zircons as well as $^{40}Ar/^{39}Ar$ thermochronology on biotites across the northern Ruby Mountains, and some samples in the lower East Humboldt Range. The fission track analyses and biotite $^{40}Ar/^{39}Ar$ yielded concordant ages from ca. 23.4 to 25.4 Ma, indicating the timing of onset of extension and the start of rapid cooling along the detachment fault.

## $^{40}Ar/^{39}Ar$ Thermochronology Results

Mineral separates (biotite and muscovite) were obtained from a total of twenty-three rock samples (sixteen from the Lamoille Canyon transect and seven from the East Humboldt Range transect) for the $^{40}Ar/^{39}Ar$ thermochronology in this study. These mineral separates were then analyzed in vacuum laser total fusion, laser step-heating and furnace step-heating experiments in the noble gas laboratory at the University of Florida. Samples were run through furnace step-

heating as well as laser step-heating due to scheduling conflicts with the laser. The methods for rough sample preparation, analytical instrumentation and procedures, and thermochronological data reduction are summarized in Appendix A.

A summary of calculated apparent ages from the $^{40}Ar/^{39}Ar$ thermochronology analyses are reported in Table 3-2. These results are organized into two groups; one corresponds to rock samples collected along the Lamoille Canyon transect and the other group to samples collected along the East Humboldt Range transect. Individual $^{40}Ar/^{39}Ar$ cooling ages are reported in Table 3-2 according to sample name, rock type, sample latitude and longitude, elevation, and the mineral that was dated. Total % $^{39}Ar$ gas used in the weighted plateau age calculation during step-heating and MSWD (mean standard weighted deviates) are also reported with the calculated cooling ages in Table 3-2. MSWD values are only relevant in step-heating age calculations, and are not reported for the laser total fusion age calculations. The higher MSWD values for some of the step-heating age calculations is generally due to the presence of excess $^{40}Ar$ in the first and last few heating steps of the experiment. However, the plateau ages are considered robust with these anomalous steps omitted. The J-values (from biotite GA1550 mineral flux monitors) used in individual cooling age calculations are also included in Table 3-2. The individual mineral cooling age spectra are shown in Figures 3-1 and 3-2.

**Biotite**

Laser step-heating experiments from two biotite separates across the East Humboldt transect resulted in mostly well-defined weighted age plateaus (Figure 3-1). Biotite from granitic gneiss sample DF02-212, yielded a flat age-plateau over 65% of the total $^{39}Ar$ gas released corresponding to an apparent age of 22.6 ± 1.2 Ma (MSWD = 3.08). Biotite from DF02-214, a biotite granite sampled from the same location as DF02-212, gave a plateau age of 24.3 ± 1.2 Ma (99% total $^{39}Ar$ gas, MSWD = 11.38).

Furnace step-heating experiments were performed on one biotite from the East Humboldt Range transect and three from the Lamoille Canyon transect. DF02-211, a biotite granite from the East Humboldt Range yielded a weighted plateau age of 23.2 ± 2.0 Ma (86% total $^{39}$Ar gas, MSWD = 2.67). DF02-205, a leucogranite, produced a weighted average age of 24.8 ± 2.7 Ma using 87% of the total $^{39}$Ar gas, with a MSWD of 15.25. The age spectrum for this biotite is internally dischordant probably because of the presence of chlorite intergrowths and $^{39}$Ar recoil. The percentage of chloritization within the DF02 biotite samples is shown in Table 3-3. DF02-206, a biotite granite yielded a flat weighted plateau age of 22.3 ± 2.6 Ma, MSWD = 9.42. Lastly, DF02-208, a biotite leucogranite from Lamoille Canyon yielded a weighted plateau age of 17.0 ± 1.6 Ma, but with only 42% of the $^{39}$Ar gas involved in the calculation, this sample was excluded from further analysis because of low total $K_2O$ and a large discordance between adjacent steps.

The higher MSWD values for samples DF02-214, DF02-205, and DF02-206 are due to the presence of excess Ar in the first few heating steps of the experiments, and chlorite intergrowths within the biotite grains. These samples were all collected from near the detachment interface and were overprinted within the greenschist facies during the formation of the retrograde mylonite. Fluid infiltration and the formation of chlorite intergrowths explains the more discordant age spectra and lower apparent $K_2O$ values of these samples.

Laser total fusion experiments and data reduction from eight biotite separates along Lamoille Canyon (separated by Virginia Newman, and analyzed by Mike Hartley) yielded ages ranging from ca. 20.7 to 31 Ma. Biotite from H97RBY-42 is a leucogranite produced an age of 31.2 ± 1.8. H97RBY-51 is a biotite garnet aplite which yielded an age of 31.3 ± 1.5 Ma. H93RBY-8 is a biotite amphibolite and yielded an age of 30.9 ± 1.8 Ma. H93RBY-4 is a biotite

granodiorite which yielded an age of 23.1 ± 1.0 Ma. H97RBY-53 is a biotite quartzite which yielded an age of 24.4 ± 0.8 Ma. H97RBY-54 is a biotite granite which yielded an age of 24.7 ± 2.2 Ma. H97RBY-55 is a mylonitic granite gneiss which yielded an age of 20.7 ± 1.0 Ma.

**Muscovite**

Muscovite separates from nine different samples collected from the two transects across the Ruby Mountains underwent in-vacuo laser and furnace step-heating $^{40}Ar/^{39}Ar$ analyses. Most of the analyses of muscovite resulted in largely well-defined, flat-shaped age spectra of better quality than the biotite analyses (Figure 3-2).

Along the Lamoille Canyon transect, five muscovite separates were analyzed. They follow a trend of younging from east to west. Three samples were analyzed using laser step-heating. DF02-216 is a leucogranite. Muscovite from this sample gave a plateau age of 32.4 ± 0.7 over 94 percent of the total $^{39}Ar$ gas released (MSWD = 0.22). Muscovite of sample DF02-218 yielded a flat age plateau over 99% of the total $^{39}Ar$ gas released and a cooling age of 32.4 ± 0.6 Ma (MSWD = 0.53). Located much further to the west, muscovite from DF02-203, a quartzite sample, yielded a plateau age of 22.6 ± 0.8 Ma (95% $^{39}Ar$ gas, MSWD = 4.32). Two samples were analyzed using furnace step-heating. DF02-209 yielded muscovite with an age of 21.7 ± 3.1 Ma with 82% of the $^{39}Ar$ gas going into the calculation and a MSWD of 7.86. DF02-210 was a quartzite sampled from the same location as DF02-209, which yielded an age of 27.9 ± 3.8 Ma (57% $^{39}Ar$, MSWD = 3.15) and a very discordant age spectrum.

Four muscovite samples from the East Humboldt Range transect were analyzed with laser step-heating and furnace step-heating methods. DF02-215 is a leucogranite located furthest west along the transect, and DF02-219 located on the furthest east side of the East Humbodlt Range along the valley between this range and the Wood Hills. Using laser step-heating, DF02-215 yielded an age of 21.5 ± 0.5 Ma with 100% of the $^{39}Ar$ gas and an MSWD of 0.23. DF02-219 is

a muscovite quartzite which yielded an age of 27.4 ± 0.6 (89% $^{39}$Ar, MSWD = 0.23). DF02-221 and H03WH-42 are samples both located in the Wood Hills, east of the Humboldt Range, and were analyzed with furnace step-heating. DF02-221 was from a quartz vein and the muscovite gave an age of 43.7 ± 5.3 Ma (89% $^{39}$Ar, MSWD = 4.50). H03WH-42 was a marble and produced an age of 49.3 ± 3.6 Ma (75% $^{39}$Ar, MSWD = 5.40).

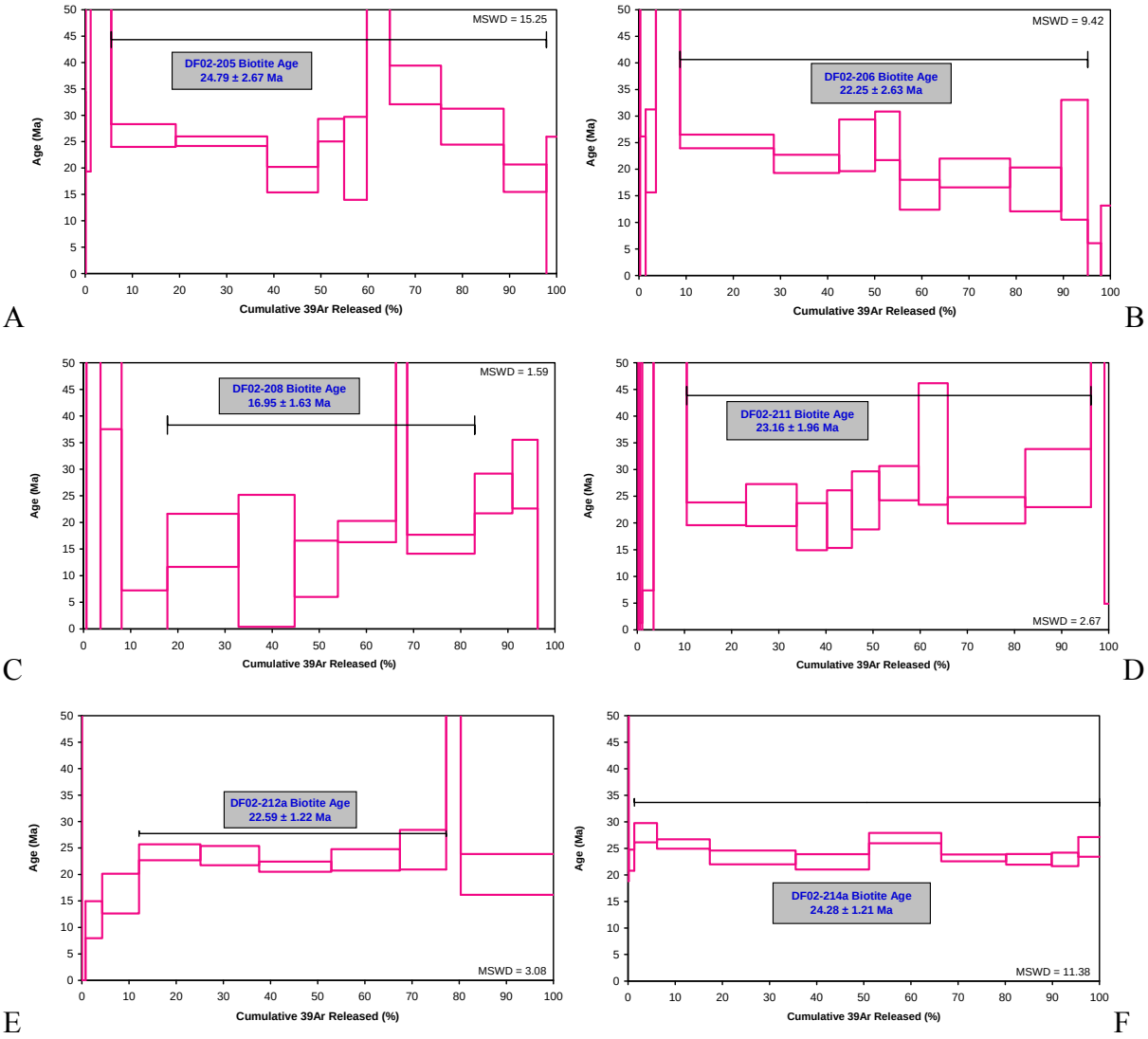


Figure 3-1. Biotite $^{40}Ar/^{39}Ar$ thermochronology step-heating mineral age ranges for samples collected from the Ruby Mountains Metamorphic Core complex along two separate transects. All ages are weighted plateau cooling ages calculated from three or more heating steps. A) DF02-205. B) DF02-206. C) DF02-208. D) DF02-211. E) DF02-212a. F) DF02-214a

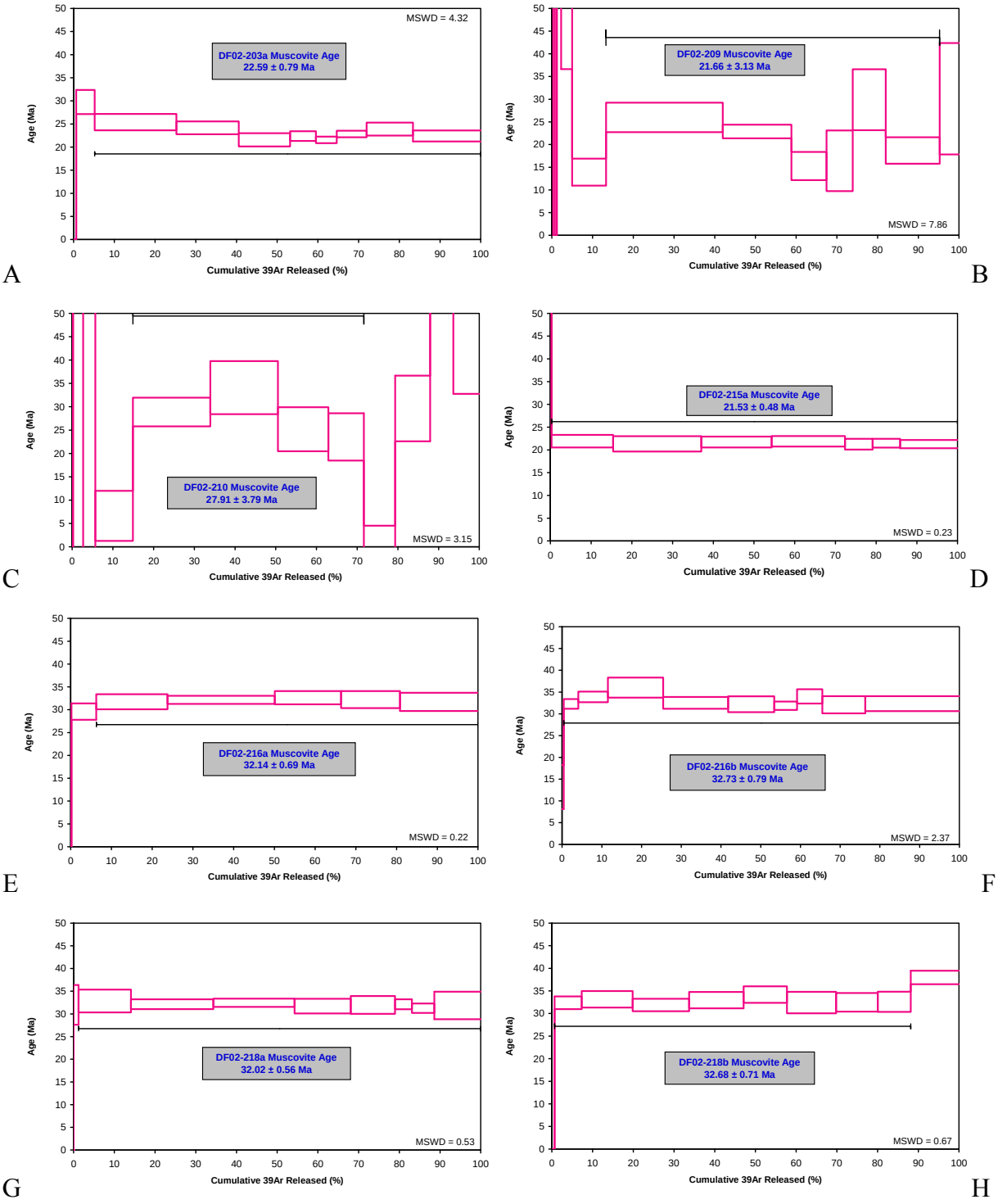


Figure 3-2. Muscovite $^{40}Ar/^{39}Ar$ thermochronology step-heating mineral age ranges for samples collected from the Ruby Mountains Metamorphic Core complex along two separate transects. All ages are weighted plateau cooling ages calculated from three or more heating steps. A) DF02-203a. B) DF02-209. C) DF02-210. D) DF02-215a. E) DF02-216a. F) DF02-216b. G) DF02-218a. H) DF02-218b. I) DF02-219a. J) DF02-219b. K) DF02-221. L) H03WH-42.

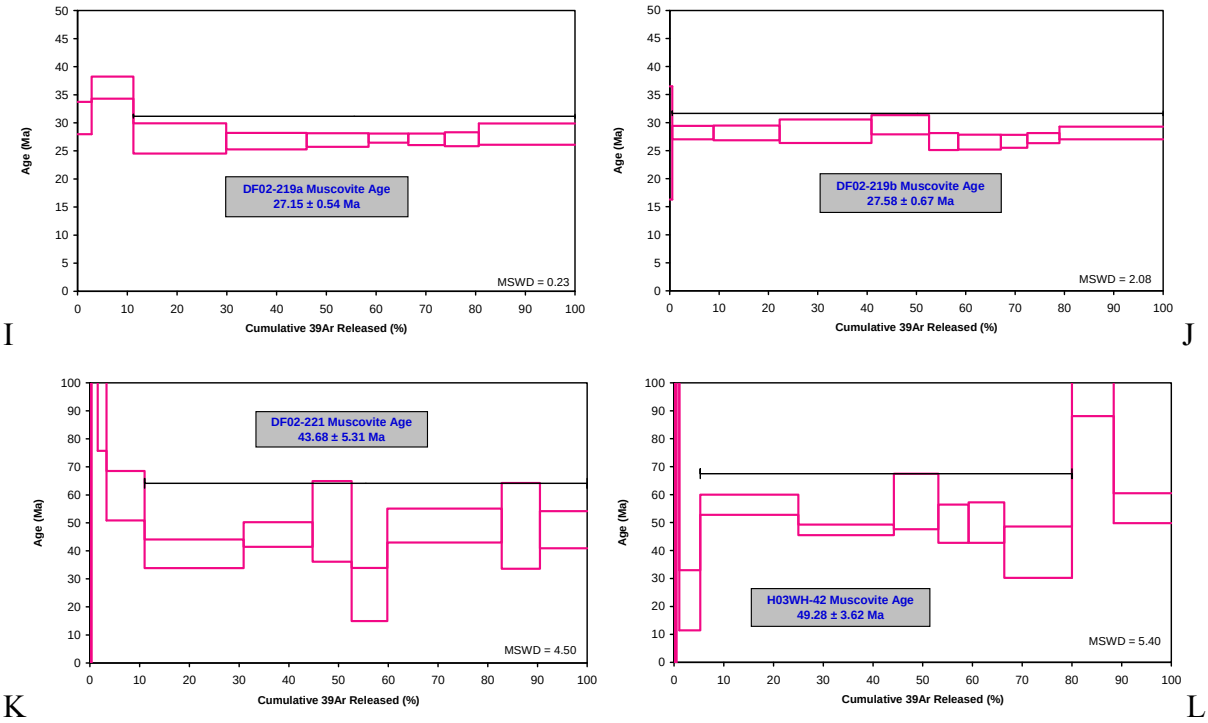


Figure 3-2. Continued.

Table 3-1. Summary of previous $^{40}Ar/^{39}Ar$ thermochronology research.

| Sample | Rock Type | Latitude | Longitude | Mineral | Age (Ma) | Errors (+/-) 2σ | Method | Source |
|---|---|---|---|---|---|---|---|---|
| Samples from $^{40}Ar/^{39}Ar$ transect in the East Humbolt Range | | | | | | | | |
| 15 | mylonitic orthogneiss | 40° 49' 44" | 115° 05' 50" | bt | 33.7 | 1.1 | Ar-Ar | Dallmeyer et al., 1986 |
| 14 | protomylonitic q dioritic orthogneiss | 40° 50' 21" | 115° 04' 46" | bt | 31.90 | 0.8 | Ar-Ar | Dallmeyer et al., 1986 |
| 4119-25 | | 40° 50' 21" | 115° 04' 46" | sphene | 23.8 | 2.5* | FT | Dokka et al., 1986 |
| 13 | protomylonitic q dioritic orthogneiss | 40° 50' 31" | 115° 04' 47" | bt | 32.9 | 0.8 | Ar-Ar | Dallmeyer et al., 1986 |
| 4119-9 | | 40° 50' 31" | 115° 04' 47" | apt | 25.1 | 4.2* | FT | Dokka et al., 1986 |
| 880805-3 | bt sill ksp pl q gar schist | 40° 56' 50" | 115° 06' 21" | bt | 26.74 | 0.08 | Ar-Ar | McGrew and Snee, 1994 |
| RM-19 | hb bt q dioritic gneiss | 40° 59' 43" | 115° 05' 26" | bt | 23.43 | 0.1 | Ar-Ar | McGrew and Snee, 1994 |
| 880709-2 | ms gar pegmatitic gneiss | 40° 59' 54" | 115° 06' 08" | ms | 21.9 | 0.2 | Ar-Ar | McGrew and Snee, 1994 |
| 880706-2A | amphibolite | 41° 00' 00" | 115° 05' 45" | bt | 21.9 | 0.2 | Ar-Ar | McGrew and Snee, 1994 |
| 870718-1 | hb bt q dioritic gneiss | 41° 00' 33" | 115° 05' 10" | bt | 20.89 | 0.1 | Ar-Ar | McGrew and Snee, 1994 |
| 870719-2B | bt monzogranitic gneiss | 41° 00' 51" | 115° 05' 25" | bt | 21.5 | 0.2 | Ar-Ar | McGrew and Snee, 1994 |
| 18 | nonmylonitic amphibolite | 41° 01' 22" | 115° 05' 52" | bt | 25.3 | 0.6 | Ar-Ar | Dallmeyer et al., 1986 |
| 870614-3 | ms bt schist | 41° 02' 05" | 115° 05' 50" | ms | 22.1 | 0.2 | Ar-Ar | McGrew and Snee, 1994 |
| 870623-2 | ms bt sill gar schist | 41° 02' 38" | 115° 06' 24" | ms | 22.2 | 0.3 | Ar-Ar | McGrew and Snee, 1994 |
| 17 | mylonitic q dioritic orthogneiss | 41° 02' 42" | 115° 00' 33" | bt | 27.7 | 0.8 | Ar-Ar | Dallmeyer et al., 1986 |
| 16 | mylonitic q dioritic orthogneiss | 41° 03' 21" | 115° 59' 55" | bt | 25.0 | 0.8 | Ar-Ar | Dallmeyer et al., 1986 |
| Samples from $^{40}Ar/^{39}Ar$ transect in the Northern Ruby Mountains | | | | | | | | |
| 5 | mylonitic quartzite | 40° 26' 20" | 115° 16' 17" | bt | 21.7 | 0.7 | Ar-Ar | Dallmeyer et al., 1986 |
| 6 | nonmylonitic mygmatitic core | 40° 46' 06" | 115° 16' 33" | bt | 22.4 | 0.7 | Ar-Ar | Dallmeyer et al., 1986 |
| 4 | nonmylonitic mygmatitic core | 40° 46' 16" | 115° 17' 38" | bt | 21.5 | 0.6 | Ar-Ar | Dallmeyer et al., 1986 |
| 5169-19 | | 40° 46' 39" | 115° 16' 21" | apt | 18.4 | 2.5* | FT | Dokka et al., 1986 |
| B | monazite-bearing bt schist | 40° 47' 21" | 115° 13' 57" | bt | 23.4 | 0.4 | K-Ar | Dallmeyer et al., 1986 |
| 8 | mylonitic q dioritic orthogneiss | 40° 49' 32" | 115° 16' 23" | bt | 22.4 | 0.8 | Ar-Ar | Dallmeyer et al., 1986 |
| 7 | mylonitic q dioritic orthogneiss | 40° 49' 54" | 115° 15' 56" | bt | 23.5 | 0.8 | Ar-Ar | Dallmeyer et al., 1986 |
| G | | 40° 51' 47" | 115° 14' 23" | bt | 13.3 | 1.0 | K-Ar | Dallmeyer et al., 1986 |
| I | ms gneiss porphyry | 40° 52' 04" | 115° 12' 42" | ms | 153.9 | 0.9 | K-Ar | Dallmeyer et al., 1986 |
| H | | 40° 52' 34" | 115° 14' 35" | bt | 15.5 | 0.4 | K-Ar | Dallmeyer et al., 1986 |
| NEV-13-80 | | 41° 03' 21" | 114° 59' 55" | apt | 26.5 | 6.3* | FT | Dokka et al., 1986 |

Table 3-1. Continued

| Sample | Rock Type | Latitude | Longitude | Mineral | Age (Ma) | Errors (+/-) 2σ | Method | Source |
|---|---|---|---|---|---|---|---|---|
| Samples from $^{40}Ar/^{39}Ar$ transect in Lamoille Canyon | | | | | | | | |
| 3 | mylonitic | 40˚ 41' 34" | 115˚ 28' 03" | bt | 20.8 | 0.5 | Ar-Ar | Dallmeyer et al., 1986 |
| 1 | nonmylonitic mygmatitic core | 40˚ 37' 41" | 115˚ 21' 58" | bt | 25.3 | 0.7 | Ar-Ar | Dallmeyer et al., 1986 |

Note: grd = granodiorite, q di = quartz diorite, gr = granite, q = quartz, bt = biotite, ms = muscovite, hbl = hornblende, ksp = potassium-feldspar, amp = amphibolite, gar = garnet, gn = gneiss, sill = sillimanite, pl = plagioclase feldspar, * sample age errors are reported at 1σ.

Table 3-2. Summary of $^{40}Ar/^{39}Ar$ thermochronology from the Ruby Mountains metamorphic core complex

| Sample | Rock Classification | Latitude | Longitude | Elevation (m) | Mineral | Age (Ma) | Errors (+/-) | % $39Ar_p$ | $MSWD_p$ | J value | Comments |
|---|---|---|---|---|---|---|---|---|---|---|---|
| Samples from the $^{40}Ar/^{39}Ar$ transect in Lamoille Canyon | | | | | | | | | | | |
| DF02-203 | 2-mica quartzite | 40˚ 41.124' | 115˚ 26.930' | 2667 | ms | 22.6 | 0.8 | 95 | 4.32 | 0.0005128 | lsh |
| DF02-205 | bt grd | 40˚ 40.024' | 115˚ 24.115' | 3059 | bt | 24.8 | 2.7 | 87 | 15.25 | 0.0036734 | fsh |
| DF02-206 | bt gr | 40˚ 38.815' | 115˚ 21.599' | 3246 | bt | 22.3 | 2.6 | 86 | 9.42 | 0.0037164 | fsh |
| DF02-208 | bt monzo-gr | 40˚ 37.628' | 115˚ 29.436' | 3290 | bt | 17.0 | 1.6 | 42 | 1.59 | 0.0038456 | fsh |
| DF02-209 | 2-mica q-rich grtd | 40˚ 37.985' | 115˚ 31.574' | 2793 | ms | 21.7 | 3.1 | 82 | 7.86 | 0.0037380 | fsh |
| DF02-210 | ms quartzite | 40˚ 37.985' | 115˚ 31.574' | 2793 | ms | 27.9 | 3.8 | 57 | 3.15 | 0.0037595 | fsh |
| DF02-216 | ms gar q syenite | 40˚ 37.267' | 115˚ 17.184' | 1957 | ms | 32.4 | 0.7 | 94 | 0.22 | 0.0005353 | lsh |
| DF02-218 | ms gar syeno-gr | 40˚ 37.539' | 115˚ 17.818' | 2093 | ms | 32.4 | 0.6 | 99 | 0.53 | 0.0005392 | lsh |
| H93RBY-4 | bt grd | 40˚ 39.278' | 115˚ 22.499' | 3039 | bt | 23.1 | 1.0 | 100 | - | 0.0060690 | ltf |
| H93RBY-8 | bt amp | 40˚ 37.661' | 115˚ 21.992' | 2561 | bt | 30.9 | 1.8 | 100 | - | 0.0060690 | ltf |
| H97RBY-42 | bt gr | 40˚ 36.765' | 115˚ 19.124' | 2088 | bt | 31.2 | 1.8 | 100 | - | 0.0060690 | ltf |
| H97RBY-51 | bt gar gr | 40˚ 35.596' | 115˚ 21.631' | 2981 | bt | 31.3 | 1.5 | 100 | - | 0.0060690 | ltf |
| H97RBY-52 | bt gn | 40˚ 37.847' | 115˚ 22.165' | 2654 | bt | 27.1 | 1.2 | 100 | - | 0.0060690 | ltf |
| H97RBY-53 | bt quartzite | 40˚ 38.926' | 115˚ 23.969' | 2310 | bt | 24.4 | 0.8 | 100 | - | 0.0060690 | ltf |
| H97RBY-54 | bt gr | 40˚ 40.461' | 115˚ 27.933' | 2010 | bt | 24.7 | 2.2 | 100 | - | 0.0060140 | ltf |
| H97RBY-55 | bt gn | 40˚ 41.500' | 115˚ 28.658' | 1905 | bt | 20.7 | 1.0 | 100 | - | 0.0060140 | ltf |
| Samples from the $^{40}Ar/^{39}Ar$ transect in the East Humbolt Range | | | | | | | | | | | |
| DF02-211 | bt granodiorite | 41˚ 01.989' | 115˚ 07.087' | 2674 | bt | 23.2 | 2.0 | 86 | 2.67 | 0.0037810 | fsh |
| DF02-212 | bt q-rich grtd | 41˚ 01.615' | 115˚ 05.996' | 2949 | bt | 22.6 | 1.2 | 65 | 3.08 | 0.0005214 | lsh |
| DF02-214 | bt monzo-gr | 41˚ 01.615' | 115˚ 05.996' | 2949 | bt | 24.3 | 1.2 | 99 | 11.38 | 0.0005300 | lsh |
| DF02-215 | ms grd | 41˚ 02.891' | 115˚ 09.392' | 2027 | ms | 21.5 | 0.5 | 100 | 0.23 | 0.0005386 | lsh |
| DF02-219 | ms quartzite | 41˚ 02.278' | 115˚ 00.313' | 1968 | ms | 27.4 | 0.6 | 89 | 0.23 | 0.0005432 | lsh |
| DF02-221 | ms quartzite | 40˚ 59.696' | 114˚ 51.282' | 2096 | ms | 43.7 | 5.3 | 89 | 4.50 | 0.0038026 | fsh |
| H03WH-42 | ms marble | 41˚ 02.105' | 114˚ 49.893' | 2211 | ms | 49.3 | 3.6 | 75 | 5.40 | 0.0038672 | fsh |

Note: grd = granodiorite, q di = quartz diorite, gr = granite, grtd = granitoid, q = quartz, bt = biotite, ms = muscovite, hbl = hornblende, kfs = potassium-feldspar, amp = amphibolite, gar = garnet, gn = gneiss, % $^{39}Ar_p$ = percent of $^{39}Ar$ used in weighted plateau age calculation, and $MSWD_p$ = mean standard weighted deviates for plateau cooling age, lsh = laser step-heating, fsh = furnace step-heating, ltf = laser total fusion. All cooling ages are reported in 2 sigma error.

Table 3-3. Summary of level of chloritization of samples from the Ruby Mountains metamorphic core complex

| Sample | Rock Classification | Mineral | % chloritization of biotite |
|---|---|---|---|
| Samples from the $^{40}Ar/^{39}Ar$ transect in Lamoille Canyon | | | |
| DF02-203 | 2-mica quartzite | ms | |
| DF02-205 | bt granodiorite | bt | 0 - 5 |
| DF02-206 | bt granite | bt | 5 - 10 |
| DF02-208 | bt monzo-granite | bt | 15 - 20 |
| DF02-209 | 2-mica q-rich granitoid | ms | |
| DF02-210 | ms quartzite | ms | |
| DF02-216 | ms gar q syenite | ms | |
| DF02-218 | ms gar syeno-granite | ms | |
| H93RBY-4 | bt granodiorite | bt | |
| H93RBY-8 | bt amphibolite | bt | |
| H97RBY-42 | bt granite | bt | |
| H97RBY-51 | bt gar granite | bt | |
| H97RBY-52 | biotite gneiss | bt | |
| H97RBY-53 | bt quartzite | bt | |
| H97RBY-54 | bt granite | bt | |
| H97RBY-55 | bt gneiss | bt | |
| Samples from the $^{40}Ar/^{39}Ar$ transect in the East Humbolt Range | | | |
| DF02-211 | bt granodiorite | bt | 10 - 15 |
| DF02-212 | bt q-rich granitoid | bt | 15 - 20 |
| DF02-214 | bt monzo-granite | bt | 0 - 5 |
| DF02-215 | ms granodiorite | ms | |
| DF02-219 | ms quartzite | ms | |
| DF02-221 | ms quartzite | ms | |
| H03WH-42 | ms marble | ms | |

Note: q = quartz, bt = biotite, ms = muscovite, hbl = hornblende, kfs = potassium-feldspar, gar = garnet

# CHAPTER 4
# DISCUSSION

## Eocene Exhumation of the Ruby Mountains Metamorphic Core Complex defined by $^{40}Ar/^{39}Ar$ Thermochronology

The $^{40}Ar/^{39}Ar$ thermochronological data obtained from rock samples collected across the Ruby Mountains define a lateral cooling age gradient, in which cooling ages young progressively to the west. Individual mineral cooling ages and transect sample localities are shown in Figure 4-1, a simplified geologic map.

Thermochronological data obtained by $^{40}Ar/^{39}Ar$ thermochronology in this study are discussed below in the context of the tectonic exhumation of the Ruby Mountains metamorphic core complex. In particular, the new thermochronologic data, combined with previous thermochronology, provide constraints on (1) the onset and duration of extension in the Ruby Mountains metamorphic core complex, and (2) the slip rate of the bounding normal detachment fault.

Samples were graphed age vs. altitude to see if there was any relationship. Based on Figure 4-2, there is no visible relationship between altitude and calculated age.

One complication for any discussion of this data is the location of the detachment fault plane. In many other metamorphic core complexes like the Harcuvar core complex in Arizona (Foster et al., 1993), physical evidence of the surface is preserved within the mountain range. This is not true for the Ruby-East Humboldt metamorphic core complex. The fault plane could have been located anywhere above the current exposure. If the fault plane was directly above the current mountain top exposures, we would have expected to see a clear pattern between the altitude of the high elevation samples and the low elevation samples compared to their calculated ages. If this were the case, the higher elevation samples would show older apparent ages, and the lower elevation samples would have passed through the closure isotherms for muscovite and

biotite at younger ages as exhumation progressed. As Figure 4-2 illustrates, there is no trend consistent with this pattern. This leads to the conclusion that the fault plane was located high enough above the current exposure that the high altitude samples had not yet passed through the biotite and muscovite Ar retention isotherms.

## Constraints on the Timing of the Onset of Extension

The method outlined by Foster and John (1999) was used to evaluate the onset of extension along the Ruby Mountains metamorphic core complex detachment fault. Figure 4-3 shows an 'age vs. distance in slip direction' graph using muscovite and biotite cooling ages ($^{40}Ar/^{39}Ar$ thermochronology) obtained from lower plate rock samples. Figure 4-2 also shows a simplified geologic map of the Lamoille Canyon area with sample locations along a projection line oriented at 285°, which is the slip direction for the detachment. The samples collected along Lamoille Canyon were input into ArcGIS, onto a geologic map, and projected orthogonally back to the slip line, defining their distances in slip direction, which are shown along the x-axis of the graph in Figure 4-3. The accuracy of this projection was estimated, and error values of ± 10 meters were assigned to the samples. The same method was used for the transect in the East Humboldt Range. The vertical error bars seen in Figures 4-3, 4-4, 4-5, and 4-6 represent the errors in the individual mica cooling ages, all calculated at 95% confidence (2 sigma).

Muscovite and biotite data were plotted together because at a cooling rate of > 25°C/m.y. the closure temperature difference is less than about 50˚C, and the error from using both types of data is, therefore, relatively small. Both muscovite and biotite cooling ages from Lamoille Canyon young in a progressive pattern towards the west across the Ruby Mountains following the direction of slip on the detachment fault system. At a distance in slip direction of ~ 12 km along the transect, mica cooling ages drop from the late Eocene (≥ 33 Ma) to the early Oligocene (≤ 25 Ma). Further west along the transect, the mica cooling ages decrease more gradually to ~

20 Ma. The change in slope of the mica cooling age curve defines the position of the mica partial argon retention zone at the onset of exhumation and the start of a period of rapid slip along the detachment fault. A regression plotted through the collection of younger samples (Figure 4-4) shows an change in slope at the 12 km mark to intersect the age line at ~ 25 Ma, indicating the age of the onset of extension in the Ruby Mountains metamorphic core complex.

The mica ages from the East Humboldt Range transect, while more sparse, are consistent with those of the Lamoille Canyon transect. There is a drop in age at ~ 27 Ma to ~24 Ma, and then a more gradual drop to ~ 21 Ma to the east along the transect. When a regression is plotted for only the younger samples (Figure 4-7), the regression line gives an age of ~ 25.5 Ma, clearly coinciding with the onset of extension in the Lamoille Canyon transect samples.

**Constraints on the Detachment Slip Rate**

Thermochronological data from rock samples collected along lower plate transects in metamorphic core complexes parallel to the direction of tectonic unroofing have also been successfully used to estimate previous slip rates on bounding detachment faults (e.g., Foster et al., 1993; Foster and John, 1999; Stockli, 2005; Wells et al., 2000). The mica ages obtained in this study likewise may be used to estimate the slip rate along the detachment fault. Slip rate estimates were made using a combination of both muscovite and biotite cooling age and distance data. To conduct these regressions, a computer program called Isoplot v. 3.09a (Ludwig, 1991) was used. Straight lines were fit to the thermochronological data using least-squares regressions. Note, samples falling into an intermediate age range (i.e., H97RBY-52, DF02-219) were excluded from both the older and younger regressions for both the Lamoille Canyon transect as well as the younger age grouping from the East Humboldt Range transect.

Figures 4-4, 4-5, and 4-7 show the results from the Isoplot least-squares regressions. For Lamoille Canyon, there were two distinct age groupings. The younger group includes eight

samples (from left to right on Figure 4-4) DF02-206, H93RBY-4, H97RBY-53, DF02-205, DF02-203, H97RBY-54, H97RBY-55, and DF02-209. The older group includes five samples (from left to right on Figure 4-5) DF02-216, DF02-218, H97RBY-42, H97RBY-51, and H93RBY-8. H97RBY-52 fell into the middle of the apparent age range and was excluded from both the older and the younger groups. The older group of samples (Figure 4-5) yielded a regression slope (m) = -0.24 ±0.22 (slope errors are 2σ). Slip rate estimates for the detachment were made from this regression by taking the inverse of the absolute values of the regression slopes and their errors (e.g., see Foster and John, 1999). The slip rate for the older group of samples was calculated to be 4.2 ±4.5 km/m.y. (or cm/yr). The younger group of samples from Lamoille Canyon (Figure 4-4) yielded a regression slope (m) = -0.24 ±0.26 (slope errors again at 2σ). The slip rate for the younger group of samples from the Lamoille Canyon transect was calculated to be 4.2 ±3.8 km/m.y. (or cm/yr).

It is important to note that the slip rate calculations are averaged over the time interval from ~ 33–30 Ma for the older Lamoille Canyon samples and ~ 26–20 Ma for the younger Lamoille Canyon samples. These ranges are the range of cooling ages used in the slip rate estimates. The slip rate calculations do not account for increases or decreases in slip along the detachment within the time interval of ~ 33–30 Ma and ~26–20 Ma (Foster and John, 1999; Stockli, 2005).

The muscovite and biotite $^{40}Ar/^{39}Ar$ data from the slightly older group of Lamoille Canyon transect samples gave apparent ages of ca. 33–31 Ma in the eastern part of the footwall. The ca. 33–31 Ma apparent age could indicate an Oligocene phase of extension at a poorly defined rate of ~ 4.2 ± 4.5 km/m.y. However, the apparent ages of these samples are all within error of each

other and could simply be due to slow cooling of the shallower part of the footwall through the biotite partial retention interval, or a crustal thermal event at about 30 Ma.

Figures 4-6 shows the mica $^{40}Ar/^{39}Ar$ ages (Ma) from the East Humboldt Range transect plotted versus their distance along slip direction (km). The group includes five samples DF02-219, DF02-212, DF02-214, DF02-211, and DF02-215, as well as 2 samples from Dallmeyer et al. (1986) and 6 samples from McGrew and Snee (1994).

It appears that the East Humboldt Range might have older and younger grouping similar to the transect in Lamoille Canyon, but the structural complexity of the region and the geographical scattering of the samples doesn't allow a regression for the data.

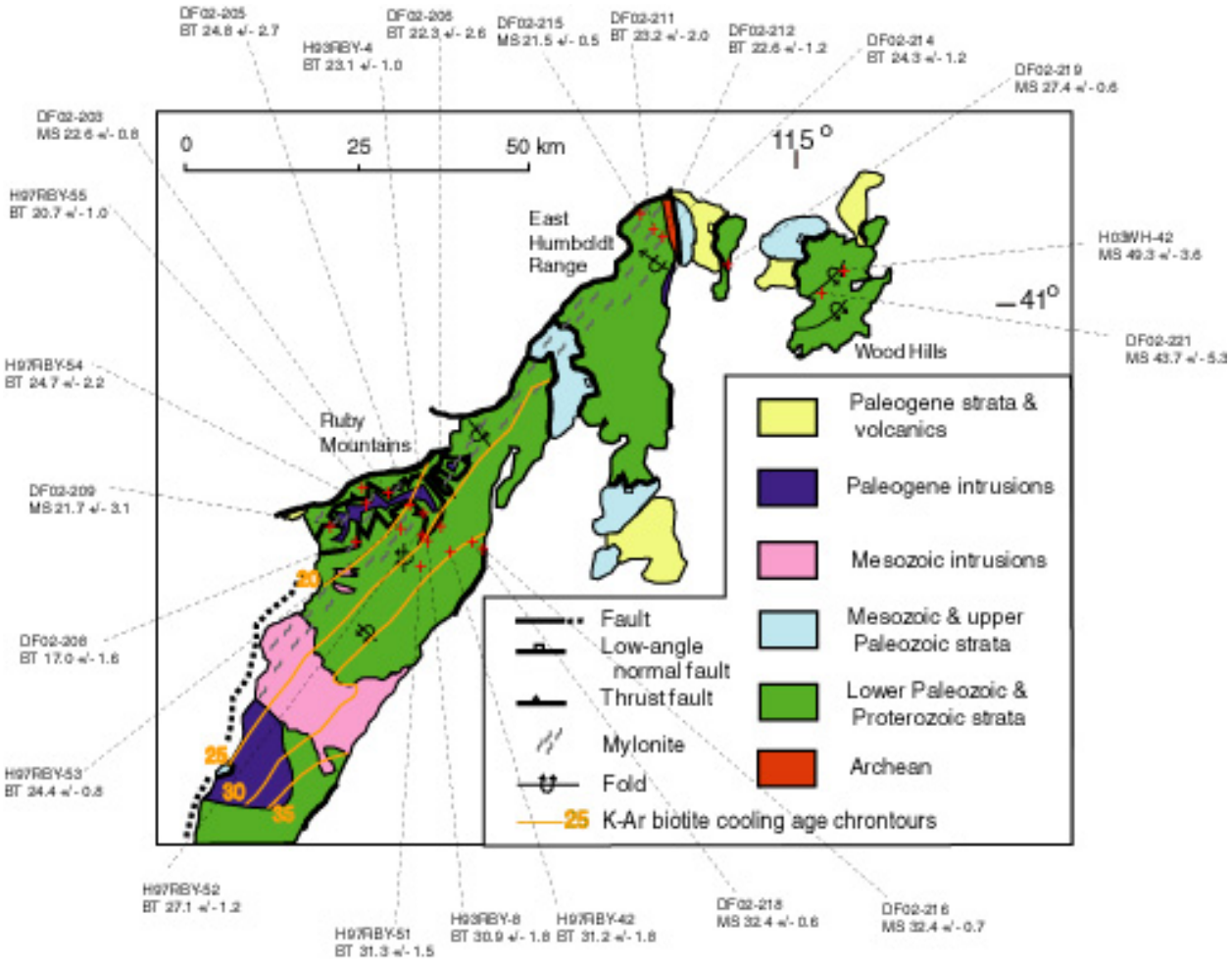


Figure 4-1. Simplified geologic map showing mineral cooling ages from samples, collected along transects across Lamoille Canyon and the East Humboldt Range, using $^{40}Ar/^{39}Ar$ thermochronology (2σ).

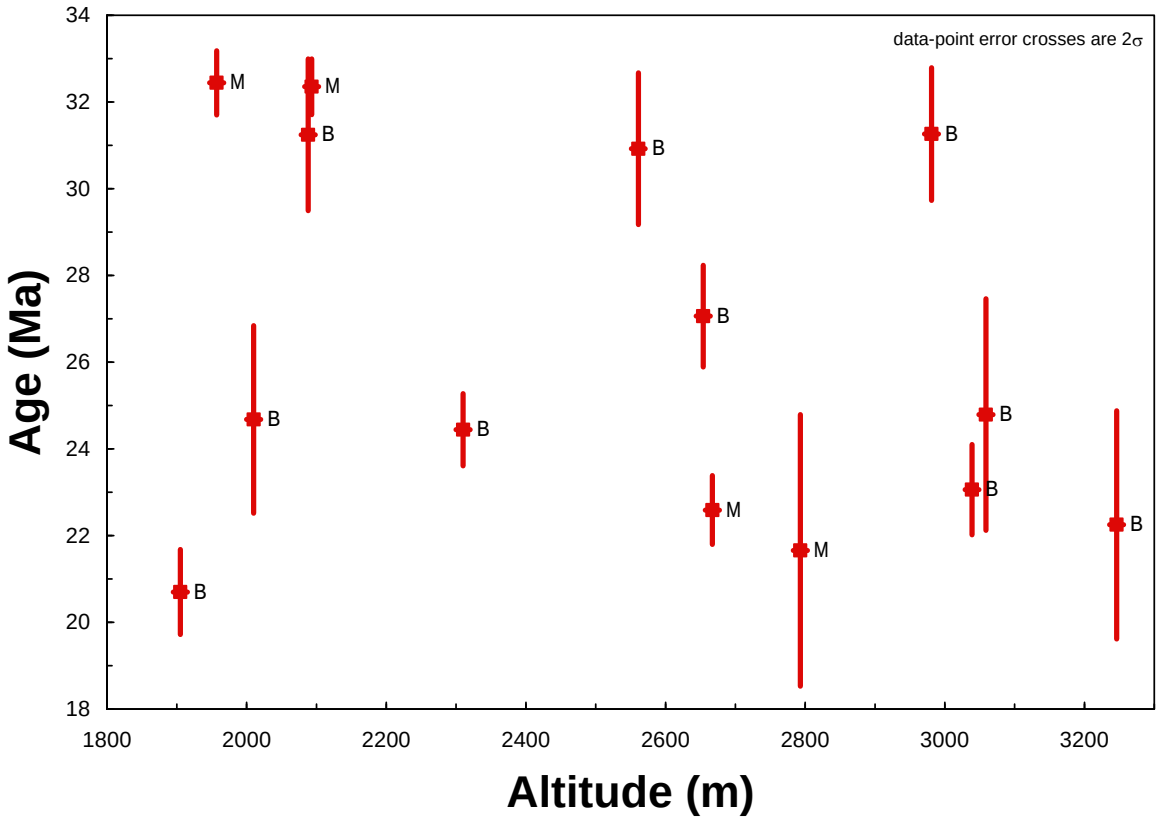


Figure 4-2. Plot of sample calculated ages vs. the altitude at which samples were collected.

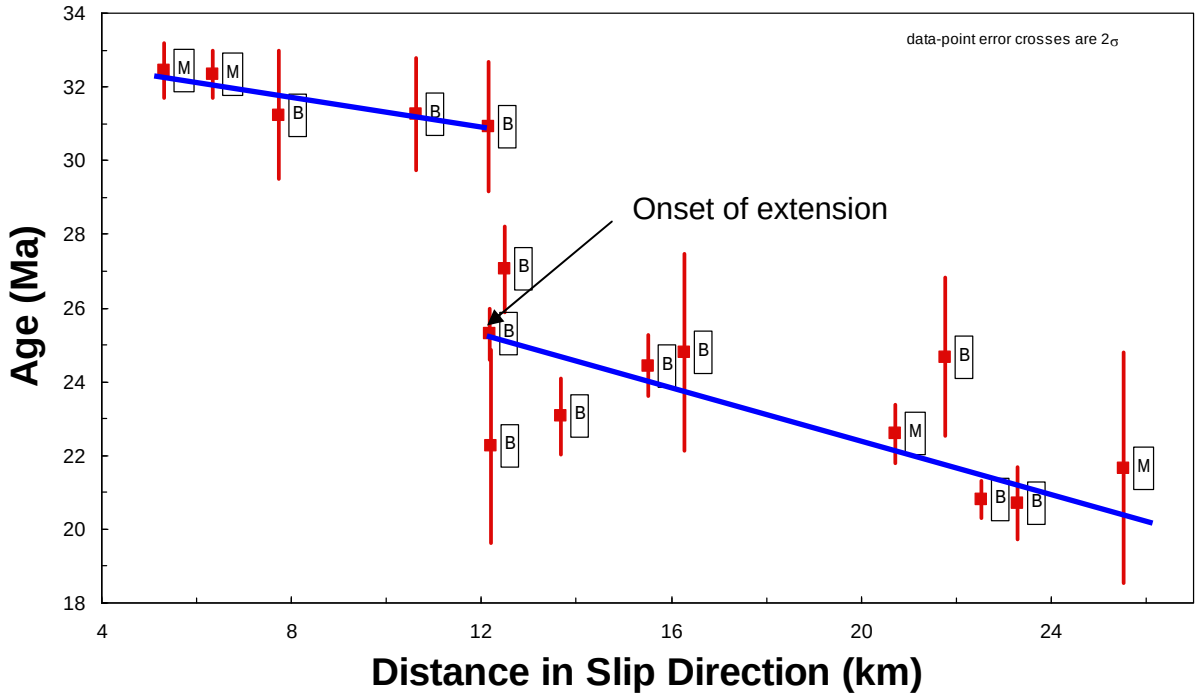


Figure 4-3. All of the mica $^{40}Ar/^{39}Ar$ thermochronology ages from the Lamoille Canyon transect were plotted versus their distance along slip direction.

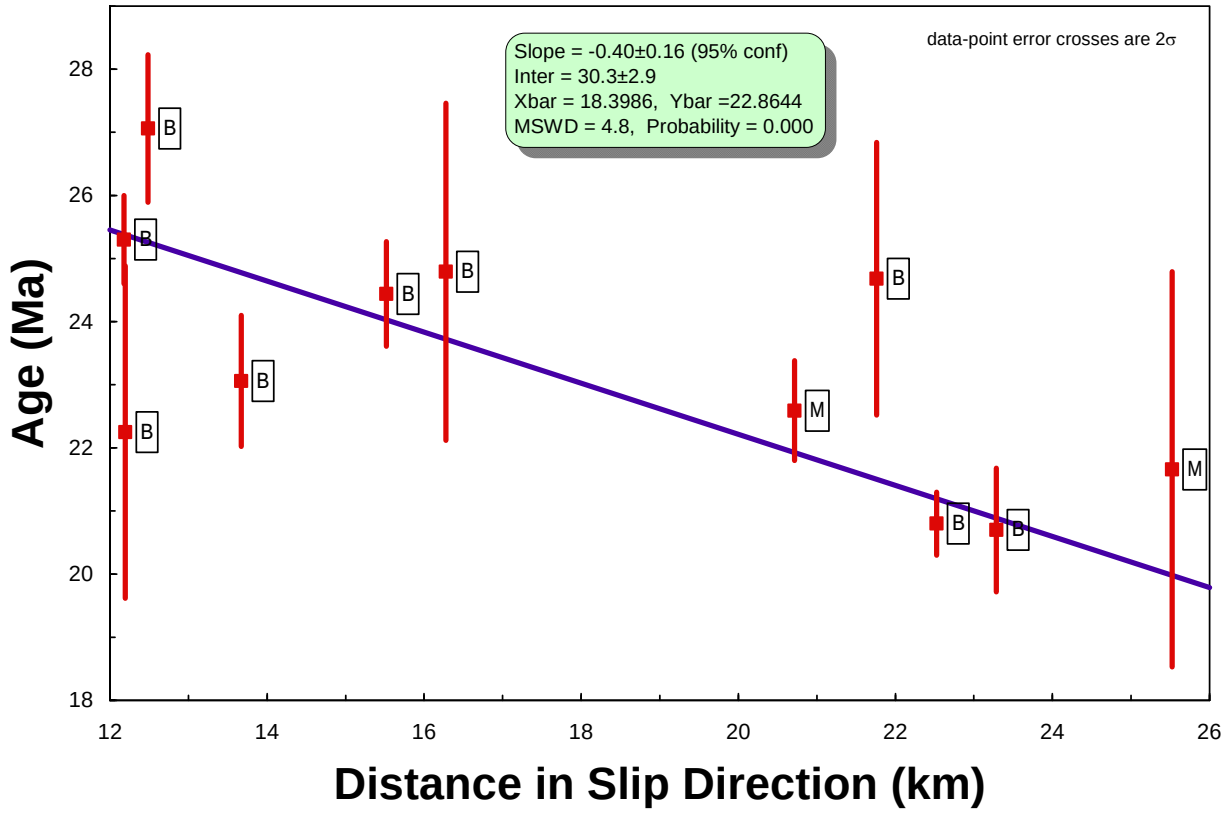


Figure 4-4. Mica $^{40}Ar/^{39}Ar$ thermochronology ages versus distance in slip direction from the Lamoille Canyon transect, younger age grouping. A regression was calculated for the sample set.

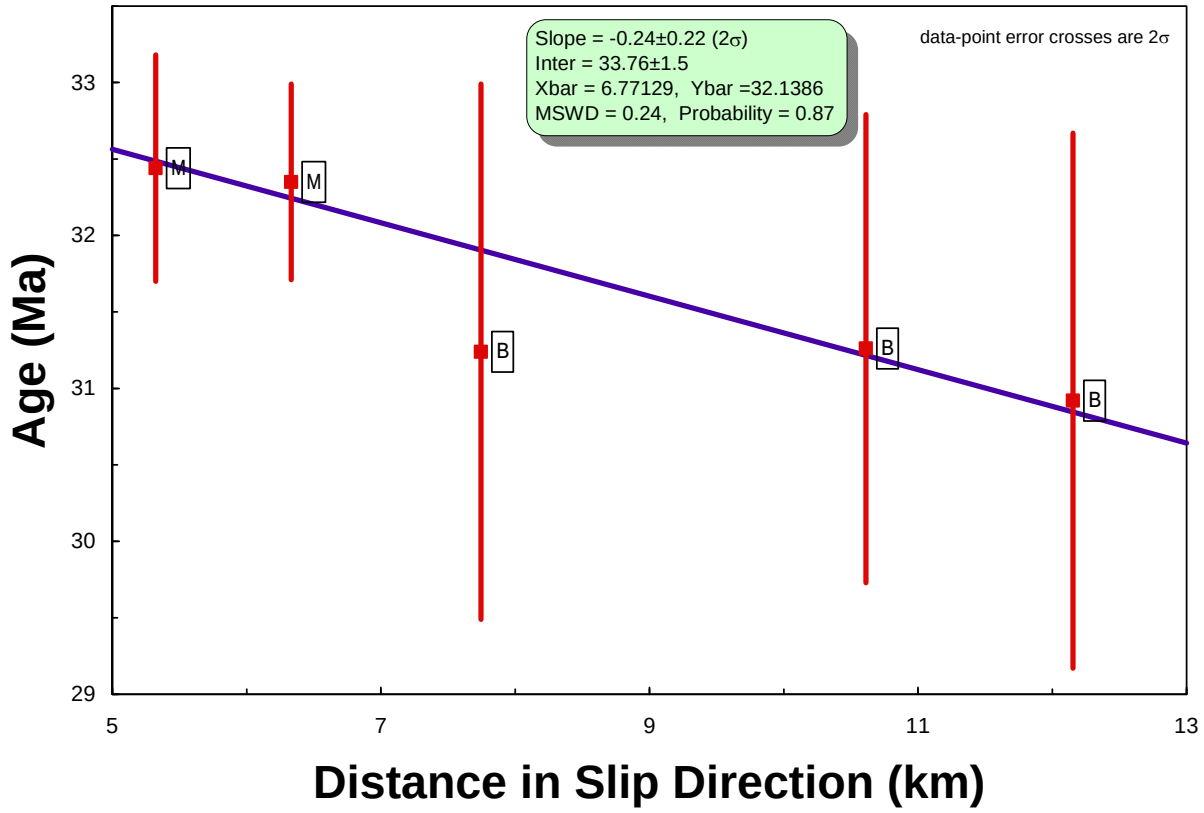


Figure 4-5. Mica $^{40}Ar/^{39}Ar$ thermochronology ages versus distance in slip direction from the Lamoille Canyon transect, older age grouping. A regression was calculated for the sample set.

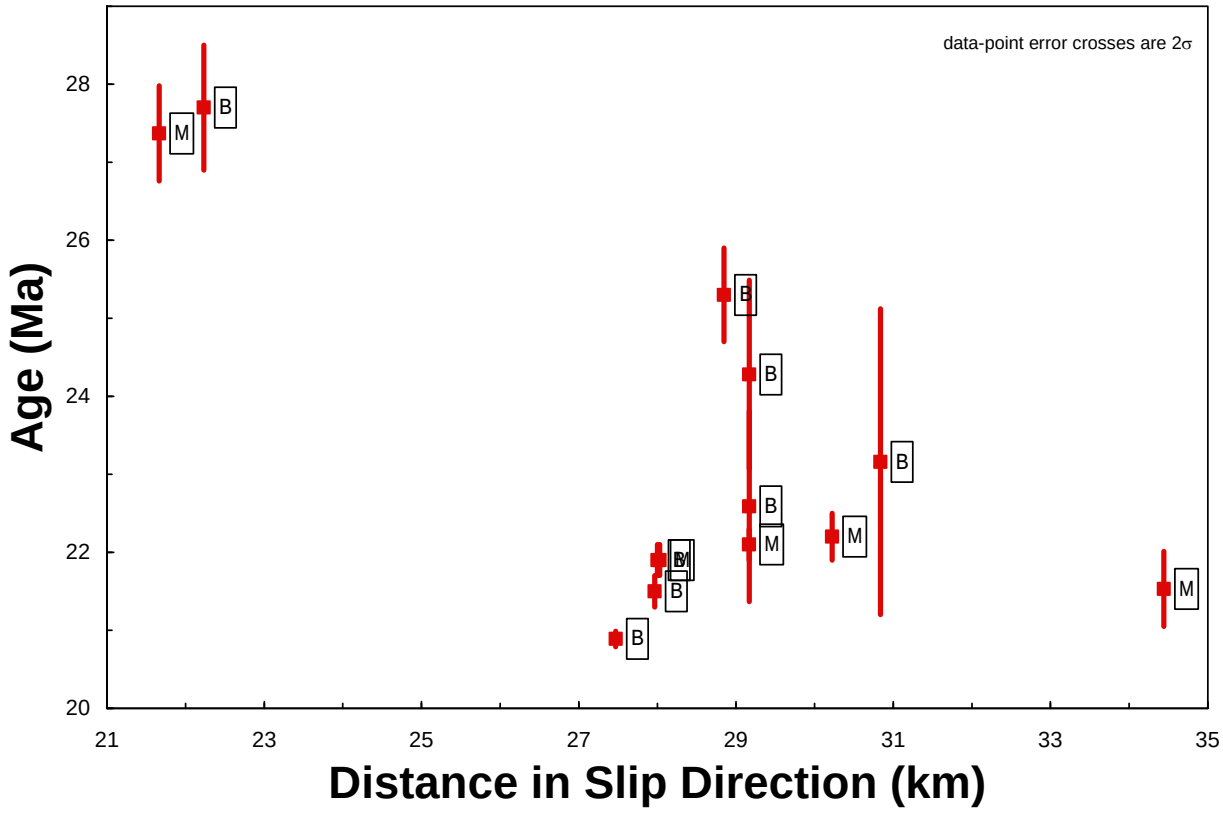


Figure 4-6. All of the mica $^{40}Ar/^{39}Ar$ thermochronology ages from the East Humboldt Range transect were plotted versus their distance along slip direction.

# CHAPTER 5
# CONCLUSIONS

The thermochronological data set obtained from the Ruby Mountains metamorphic core complex transect across Lamoille Canyon shown in this study provide several constraints on the exhumation onset and slip rate during the Eocene and Miocene: (1) The age of the onset of extension in the Ruby Mountains is indicated to be ~25 Ma by the marked break in the slope of the cooling age curve on the age vs. distance diagram constructed from the mica cooling ages (Fig. 4-3). This thermochronology-based age constraint is in good agreement with the previous thermochronology done in the area (e.g., Dallmeyer et al., 1986; Dokka et al., 1986; Howard, 2003; McGrew and Snee, 1994). Thus, the onset of extension in the Ruby Mountains is now well constrained and confirmed to be at ~ 25 Ma. Furthermore, (2) the cooling ages from micas show that extension in the Ruby Mountains across Lamoille Canyon continued until at least ~ 20 Ma. (3) Muscovite and biotite $^{40}Ar/^{39}Ar$ thermochronological data obtained during this study were also used to constrain the slip rate on the detachment fault. These data show that between ~ 26–18 Ma, the averaged slip rate on the detachment was ~ 4.2 ± 3.8 km/m.y. (4) $^{40}Ar/^{39}Ar$ data from the eastern part of the footwall may indicate an Oligocene phase of extension at a rate of ~ 4.2 ± 4.5 km/m.y. (or cm/yr) from ~ 33–31 Ma, or record the graduate cooling before the onset of extension.

# APPENDIX
# $^{40}Ar/^{39}Ar$ THERMOCHRONOLOGY METHODS

## Sample Preparation and Irradiation

20 samples were collected along two transects in 2002. Billets were cut from the samples and were sent to Texas Petrographic Inc. to be cut and polished into thin sections. Examination of the thin sections provided information on the extent of alteration to various mineral phases in the rock samples to be used in $^{40}Ar/^{39}Ar$ analyses. Samples that showed un-altered micas, K-feldspars, and hornblende were selected for mineral separation and $^{40}Ar/^{39}Ar$ analyses.

The selected samples were crushed and milled into a sand sized fraction using a Sturtevant rock Jaw Crusher and Bico Pulverizer type UA disk mill. The pulverized sample was sieved. Each sample was then run through the water table to separate minerals according to density. The IV and III (lightest) water table fractions were used further to process for K-feldspar and muscovite, and the water table II and I fractions were processed for biotite and hornblende.

Following water table processing, tetrabromoethane (TBE) and methylene iodine (MI) heavy liquids (densities of 2.96 and 3.33 g/cm3, respectively) were used to separate the micas, K-feldspar, and hornblende from less dense minerals. These separates were rinsed with ethanol (for TBE) and acetone (for MI) 2-3 times following separation. Special dilute TBE mixes were used to further separate the TBE floats (containing quartz, K-feldspar, plagioclase feldspar, muscovite, etc.) to first sink the quartz and feldspars and allow the muscovite to float, and then to sink the quartz and plagioclase feldspar and allow the K-feldspar to float.

A Frantz magnetic separator Model L-1 was used to separate the biotite and hornblende from non-magnetic phases. Only the most magnetic biotite and hornblende Frantz separates were kept to avoid inclusion-rich minerals. All mineral separates were then hand picked under a binocular microscope for better refinement using standard picking tools (i.e., nylon brushes,

Pyrex© glass dishes, and wax weighing paper). Some separates were given an ultrasonic bath in de-ionized water for approximately fifteen minutes to remove any altered materials.

Nine muscovite separates and seven biotite separates along with GA1550 biotite flux monitors (98.79 ± 0.5 Ma, see Reene et al., 1998) were individually packaged in aluminum foil (~ 5 mg for mineral separate, ~ 1 mg for flux monitors) and sealed in a pure quartz glass. The mineral separates and flux monitors were irradiated in 2 different batches in a 1.1 MW TRIGA MARK II research nuclear reactor at the Oregon State University Radiation Center. For a more detailed description of these facilities and irradiation methods see http://ne.oregonstate.edu/facilities/radiation_center/. The first batch, OS10, was irradiated for 2 hours. This included samples: DF02-203 (muscovite), DF02-212 (biotite), DF02-214 (biotite), DF02-215 (muscovite), DF02-216 (muscovite), DF02-218 (muscovite), and DF02-219 (muscovite). The second batch, OS11, was irradiated for 7 hours and included samples DF02-204 (biotite), DF02-205 (biotite), DF02-206 (biotite), DF02-208 (biotite), DF02-209 (muscovite), DF02-210 (muscovite), DF02-211 (biotite), DF02-221 (muscovite), and H03WH-42 (muscovite).

## $^{40}Ar/^{39}Ar$ Analytical Instrumentation and Procedures

The $^{40}Ar/^{39}Ar$ analyses were carried out in the noble gas laboratory at the Department of Geological Sciences, University of Florida. A combination of both laser ablation step-heating and furnace step-heating techniques were utilized to extract Ar gas from mineral separates. Laser ablation step-heating of mica separates was done by a water-cooled New Wave Research model MIR10 30W $CO_2$ laser. During laser step-heating the New Wave laser was manually controlled using LAS (laser ablation software) version 1.3.0.1 by New Wave Research. Mica separates were ablated a total of 5-15 steps under a 1750 μm continuous wavelength focused laser beam at 2-5.5% power. A final laser fusing-step was done at 10-12% power. The step-

heating schedule used for laser ablation varied and was adjusted accordingly to maximize Ar gas output for the mineral separates.

A water-cooled, double vacuum, resistively heated furnace was used to step-heat the remaining mica separates. The furnace step-heating analyses were controlled automatically. The heating schedule was programmed into the computer to maximize the Ar gas output for each heating step ranging from a de-gassing step at 400 degreed to a fusing step at 1450 degrees.

Ar gas extracted from mineral samples by laser and furnace step-heating was transferred by vacuumed lines to a getters trap for 10 minutes to remove reactive gasses. The purified Ar gas was analyzed in a gas-sourced Mass Analyzer Products Model 215-50 mass spectrometer equipped with a filament for gas ionization and a magnetic sector mass discriminator followed by a Balzers Electron Multiplier collector to measure the isotopic abundances of $^{36}Ar$, $^{37}Ar$, $^{38}Ar$, $^{39}Ar$, and $^{40}Ar$. Cold laser blanks were analyzed at the beginning of each analytical session and every five steps after. The laser blanks were obtained by closing the laser chamber for two minutes and then passing the blank gas to the mass spectrometer following the same steps as a regular sample step. Heated furnace blanks were made by closing and heating the empty furnace to 400°C, 600°C, 800°C, 1000°C, 1200°C and 1450°C prior to sample step-heating.

Data files produced from the mass spectrometer sample and blank analyses were imported into the program ArArCALC version 2.4 by Koppers (2002) for data reduction and $^{40}Ar/^{39}Ar$ cooling age calculations. ArArCALC uses Microsoft Excel© to plot data tables, age plateaus and isochrons. ArArCALC was also used to calculate J-values from laser total fusion analyses of the GA1550 biotite flux monitors. These J-values were then applied to their individual samples to better constrain their $^{40}Ar/^{39}Ar$ cooling age calculations.

LIST OF REFERENCES

Angelier, J., and Coletta, B., 1983, Tension fractures and extensional tectonics: Nature, v. 301, p. 203–222.

Armstrong, R.L., and Ward, P., 1991, Evolving geographic patterns of Cenozoic magmatism in the North American cordillera: The termoral and spatial association of magmatism and metamorphic core complexes: Journal of Geophysical Research, v. 96, p. 13,201–13,224.

Brun, J., Sokoutis, D., and Driessche, J. V. D., 1994, Analogue modeling of detachment fault systems and core complexes: Geology, v. 22, p. 319–322.

Buck, W.R., 1988, Flexural rotation of normal faults: Tectonics, v. 7, p. 959–973.

Burchfiel, B.C., Cowan, D.S., Davis, G.A., 1992, Tectonic Overview of the Cordilleran Orogen in the Western United States: The Geology of North America, The Geological Society of America, v. G-3, p. 407–479.

Carter, T.J., Kohn, B.P., Foster, D.A., and Gleadow, A.J.W., 2004, How the Harcuvar Mountains metamorphic core complex became cool: Evidence from apatite and (U-Th)/He thermochronometry: Geology, v. 32, p. 985–988.

Chery, J., 2001, Core complex mechanics: From the Gulf of Corinth to the Snake Range: Geology, v. 21, p. 439–442.

Coney, P.J., 1980, Cordilleran metamorphic core complexes: An overview: Geological Society of America, Memoir 153, p. 7–31.

Dallmeyer, R.D., Snoke, A.W., and McKee, E.H., 1986, The Mesozoic-Cenozoic Tectonothermal evolution of the Ruby Mountains, East Humboldt Range, Nevada: a cordilleran metamorphic core complex: Tectonics, v. 5, p. 931–954.

Davis, G.H., 1983, Shear-zone model for the origin of metamorphic core complexes: Geology, v. 11, p. 342–347.

Dokka, R.K., Mahaffie, M.J., Snoke, A.W., 1986, Thermochronologic evidence of major tectonic denudation associated with detachment faulting, northern Ruby Mountains-East Humboldt Range, Nevada: Tectonics, v. 5, p. 995–1006.

Foster, D.A., Gleadow, A.J.W., Reynolds, S.J., Fitzgerald, P.G., 1993, Denudation of metamorphic core complexes and the reconstruction of the transition zone, West Central Arizona: Constraints from apatite fission track thermochronology: Journal of Geophysical Research, v. 98, p. 2167–2185.

Foster, D.A., and John, B.E., 1999, Quantifying tectonic exhumation in an extensional orogen with thermochronology: examples from the southern Basin and Range Province: In Ring, U., Brandon, M., Lister, G.S., and Willett, S.D. (eds), Exhumation Processes: normal faulting, ductile flow, and erosion: Geological Society (London) Special Publication, 154, p. 356–378.

Grice, W., 2006, Exhumation and cooling history of the middle Eocene Anaconda metamorphic core complex, western Montana: Master of Science Thesis Defense, University of Florida.

Henry, C.D., and Boden, D.R., 1998, Eocene Magmatism: The heat source for Carlin-type gold deposits of northern Nevada: Geology, v. 26, p. 1067–1070.

Hofstra, A.H., and Cline, J.S., 2000, Characteristics and models for Carlin-type gold deposits: Reviews in Economic Geology, v. 13, p. 163–220.

Howard, K.A., 1980, Metamorphic infrastructure in the Northern Ruby Mountains, Nevada: Geological Society of America, Memoir 153, p. 335–347.

Howard, K.A., 2003, Crustal structure in the Elko-Carlin region, Nevada, during Eocene gold mineralization: Ruby-East Humboldt metamorphic core complex as a guide to the deep crust: Economic Geology, v. 98, p. 249–268.

Kistler, R.W., Ghent, E.D., O'Neil, J.R., 1981, Petrogenesis of garnet two-mica granites in the Ruby Mountains, Nevada: Journal of Geophysical Research, v. 86, p. 10,591–10,606.

Koppers, A.A.P., 2002, ArArCALC - software for Ar-40/Ar-39 age calculations: Computers and Geosciences, v. 28, p. 605–619.

Lister, G.S., and Davis, G.A., 1989, The origin of metamorphic core complexes and detachment faults formed during Tertiary continental extension in the northern Colorado River region, USA: Journal of Structural Geology, v. 11, p. 65–94.

McDougall, I., and Harrison, T.M., 1999, Geochronology and Thermochronology by the $^{40}Ar/^{39}Ar$ method, 2nd edition. Oxford University Press, N.Y.

McGrew, A.J., and Snee, L.W., 1994, $^{40}Ar/^{39}Ar$ thermochronologic constraints on the tectonothermal evolution of the northern East Humboldt Range metamorphic core complex, Nevada: Tectonophysics, v. 238, p. 425–450.

Miller, E.L., Dumitru, T.A., Brown, R.W., and Gans, P.B., 1999, Rapid Miocene slip on the Snake Range-Deep Creek Range fault system, east-central Nevada: Geological Society of America Bulletin, v. 111, p. 886–905.

Oldow, J.S., 1984, Evolution of a late Mesozoic back-arc fold and thrust belt, northwestern Great Basin, U.S.A.: Tectonophysics, v. 102, n. 1–4, p. 245–274.

Poole, F.G., 1992, Distribution and thickness of late Proterozoic through middle Ordovician rocks: The Geology of North America, The Geological Society of America, vol. G-3, p. 407–479.

Roberts, R.J., Ferguson, H.G., Gilluly, J., Hotz, P.E., 1958, Paleozoic rocks of north-central Nevada: Bulletin of the American Association of Petroleum Geologists, v. 42, n. 12, p. 2813–2857.

Snoke, A.W., 1980, Transition from infrastructure to suprastructure in the northern Ruby Mountains, Nevada: Geological Society of America, Memoir 153, p. 287–333.

Stockli, D.F., 2005, Application of low-temperature thermochronometry of extensional tectonic settings: Reviews in Mineralogy and Geochemistry, v. 58, p. 411–448.

Wells, M.L., Snee, L.W., and Blythe, A.L., 2000, Dating of major normal fault systems using thermochronology: An example from the Raft River Mountains, Basin and Range, western United States: Journal of Geophysical Research, v. 105, p. 16,303–16,327.

Wernicke, B., 1981, Low-angle faults in the Basin and Range province: Nappe tectonics in an extending orogen: Nature, v. 291, p. 645–648.

Wernicke, B., 1985, Uniform-sense normal simple shear of the continental lithosphere: Canadian Journal of Earth Sciences, v. 22, p. 108–126.

Wernicke, B., and Axen, G. J., 1988, On the role of isostasy in the evolution of normal fault systems: Geology, v. 16, p. 848–851.

# BIOGRAPHICAL SKETCH

Jennifer was born in Hartford, CT, in 1983. She is the youngest of three sisters. She graduated from RHAM high school (Hebron, CT) in 2001. She received a Bachelor of Science degree in geology from Syracuse University (Syracuse, NY) in 2005. While attending graduate school at the University of Florida (Gainesville, FL), Jennifer served as a teaching assistant for several courses in the Department of Geological Sciences and as a research assistant for Dr. David A. Foster. She received a master's degree in geology from the University of Florida in May of 2008. Jennifer continues to pursue her interests in the PhD program in geology at the University of Florida (Gainesville, FL).

# QUANTIFYING EOCENE AND MIOCENE EXTENSION IN THE SEVIER HINTERLAND IN NORTHEASTERN NEVADA

Jennifer N. Gifford
Geological Sciences
David A. Foster
Master of Science
May 2008

This project provides a comprehensive low-temperature thermochronologic history of the Ruby Mountain metamorphic core complex in northeast Nevada, and helps to define the Tertiary extensional history of the region. Samples from two transects across the range were analyzed using furnace and laser $^{40}Ar/^{39}Ar$ methods. Data generated by this project was used to: a) establish the timing of Paleogene and Neogene exhumation and rate of westward slip on the fault system that separates the upper crustal block that include the Carlin gold trend mineralizations from the Ruby Mountains metamorphic core complex, and b) better understand the geologic setting and origin of the Carlin-type deposits that form the Carlin gold trend.